applied sciences

MDPI

Article

Deep Learning-Based Receiver for Low-Complexity 6G Partial LIS Architectures

Mário Marques da Silva [1,2,3,4,*], Héctor Orrillo [1,2,4] and Rui Dinis [2,3,5]

1 Department of Engineering and Computer Sciences, Universidade Autónoma de Lisboa, 1169-023 Lisboa, Portugal; horrillo@autonoma.pt
2 Autonoma TechLab, 1169-023 Lisboa, Portugal; rdinis@fct.unl.pt
3 Instituto de Telecomunicações, 1049-001 Lisboa, Portugal
4 Ci2—Centro de Investigação em Cidades Inteligentes, 2300-313 Tomar, Portugal
5 Faculty of Sciences and Technology, Universidade Nova, 2829-516 Caparica, Portugal
* Correspondence: mmsilva@autonoma.pt

Abstract

The sixth generation (6G) of wireless networks demands extreme energy efficiency and massive connectivity, positioning large intelligent surfaces (LIS) as a pivotal technology. However, the practical deployment of LIS is constrained by the overwhelming computational complexity and power consumption required to process thousands of antenna elements. To address these challenges, this article proposes a deep learning-based receiver architecture that integrates the spatial efficiency of Partial LIS with advanced non-linear detection. By activating only a subset of antenna panels closest to the user terminal (Partial LIS), the system significantly reduces hardware overhead and Radio Frequency (RF) power consumption. To compensate for the performance loss, the multi-user interference (MUI) generated by the linear combining stage, and the increased MUI inherent in a reduced-aperture environment, a specialized Multilayer Perceptron (MLP) network is implemented. Unlike traditional Zero-Forcing (ZF) or Minimum Mean Squared Error (MMSE) receivers, which require energy-intensive matrix inversions for each frequency component, the proposed neural-network-enabled receiver achieves near-optimal performance using low-complexity combining followed by intelligent learning-based interference suppression. Simulation results demonstrate that the proposed hybrid architecture provides a scalable, "green" solution for 6G uplink scenarios. Notably, the deep learning approach is shown to effectively suppress the performance loss of reduced apertures, achieving a BER comparable to traditional linear benchmarks even with a reduced physical aperture, maintaining good Bit Error Rate (BER) performance while dramatically reducing the computational and hardware footprint.

Keywords: 6G; large intelligent surfaces (LIS); Partial LIS; neural networks; multi-user interference; SC-FDE

Academic Editor: Mirosław Klinkowski

Received: 26 February 2026
Revised: 28 March 2026
Accepted: 30 March 2026
Published: 1 April 2026

1. Introduction

According to the recent ITU-R M.2160-0 framework, sixth-generation (6G) systems (IMT-2030) are expected to significantly outperform 5G (fifth-generation) benchmarks, with research targets for peak data rates reaching up to several hundred Gbps (and potentially 1 Tbps in specific high-capacity scenarios) and user-experienced data rates aiming for the 1 Gbps mark [1].

Achieving these targets requires energy and spectral efficiencies 10 to 100 times and 5 to 10 times better than those of 5G [2]. While 5G relies on mm-Wave and massive MIMO (Multiple Input Multiple Output), 6G must incorporate new frequency bands, such as Visible Light Communications (VLCs) and Terahertz bands (100 GHz–10 THz), alongside revolutionary concepts like large intelligent surfaces (LIS) [2–6]. These smart radio environments, empowered by reconfigurable meta-surfaces, allow for a proactive control of the wireless propagation channel [6]. Recent studies have highlighted that LIS can provide holographic MIMO capabilities for 6G networks, although this introduces significant challenges in terms of channel modeling under Rayleigh fading and spatial consistency [4,5]. However, the practical implementation of LIS is hindered by the massive computational overhead and power consumption required to process hundreds or thousands of antenna elements. LIS systems operate predominantly in short-range and near-field conditions, utilizing a high number of antenna elements with tight spacing (typically $\lambda/2$). This allows the entire LIS array to act like a lens, providing distance-dependent focusing [7–9], much like a magnifying glass focusing sunlight. This 'Beyond Massive MIMO' capability enables LIS to suppress interference between users located in the same direction but at different distances, a feat traditional beamforming cannot achieve.

Two specific strategies were proposed in our previous research to address these issues. In [10], we introduced the concept of Partial LIS, demonstrating that activating only a subset of antenna panels, those closest to the user terminal, can significantly reduce complexity and power consumption while maintaining a good level of performance. This approach directly addresses the hardware-level challenges of massive surfaces. On the signal processing front, the use of Single-Carrier with Frequency-Domain Equalization (SC-FDE) is an efficient modulation for the uplink of such systems due to the reduced Peak-to-Average Power Ratio (PAPR) [11], typically coupled with low-complexity receivers like Maximum Ratio Combining (MRC) and Equal Gain Combining (EGC) [12,13].

More recently, in [14], we addressed the receiver's limitations by proposing a neural-network-based (NN) post-detection interference suppression scheme for LIS systems. The approach of using MRC and EGC iterative receivers, associated with LIS systems, is computationally efficient but typically suffers from residual interference compared to Zero-Forcing (ZF) or Minimum Mean Squared Error (MMSE) detectors [10,14]. The performance gap between these techniques stems from a fundamental architectural difference: while ZF and MMSE process all users simultaneously to decouple their signals through matrix inversion, MRC and EGC treat each user independently. Consequently, they fail to nullify the cross-user contributions, leading to a residual interference floor that limits the system's capacity as the signal power increases.

Building upon these foundations, this article differentiates itself from previous works by addressing a critical gap: the performance floor that arises in Partial LIS due to increased spatial correlation and multi-user interference (MUI). While [10] focused on hardware selection and [14] applied NNs to Full LIS architectures, the novelty of this work lies in the specialized synthesis of a shallow MLP receiver specifically trained to suppress the non-linearities unique to the reduced-aperture Partial LIS. This allows us to achieve a 75% reduction in RF complexity while maintaining the detection accuracy of high-complexity matrix-inversion-based receivers, a trade-off and computational mapping not previously explored.

Recent advancements have demonstrated its effectiveness in diverse applications, ranging from non-destructive monitoring technologies in agriculture [15] to fault prediction methods in mechanical systems using digital twins and transfer learning [16]. The potential of deep learning (DL) to address complex non-linearities is well-documented, with recent advancements in 6G architectures ranging from hybrid precoding in TeraHertz communications [17] to optimized antenna selection [18]. Specific research into near-field beamforming has also demonstrated that learning-based models can effectively handle spherical wavefronts [19,20]. Building on this, our proposed unified hybrid framework integrates the structural efficiency of Partial LIS [10] with a specialized one-shot (non-iterative) MLP receiver.

While [10] established the modular architecture and [14] explored NN receivers for full apertures, this work focuses on the unique synergy required for a reduced active aperture. The proposed NN is specifically trained to suppress the residual MUI and nonlinearities resulting from the lower spatial resolution of a single active panel. By combining these approaches, we deliver a system that maximizes energy and computational efficiency while maintaining a robust Bit Error Rate (BER) performance, closely approaching the full-aperture linear baseline.

The remainder of this article is organized as follows: Section 2 describes the system model and the characterization of the LIS-based uplink environment. Section 3 details the proposed hybrid architecture, including the selective panel activation mechanism (Partial LIS) and the design of the Multilayer Perceptron (MLP)-based interference suppression module. Section 4 presents and discusses the simulation results, comparing the performance of the proposed solution against several benchmarks under different antenna resolutions and user loads. Finally, Section 5 concludes the paper by summarizing the main findings and discussing future research directions.

2. System Characterization

In this section, we describe the uplink transmission model using SC-FDE integrated with a Partial LIS architecture and the proposed NN-based receiver.

2.1. Transmitted Signal and Channel Model

Consider a multi-user uplink scenario where U single-antenna users transmit signals to a LIS composed of N total antenna elements, organized into multiple panels. The transmission employs SC-FDE modulation with K subcarriers. The time-domain data block for the u-th user is denoted by the vector $\mathbf{s}_u$; after the addition of a cyclic prefix at the transmitter and a Discrete Fourier Transform (DFT) operation at the receiver side, the corresponding frequency-domain received signal is represented by $S_u(k)$ for the k-th subcarrier. As a general notation rule throughout this paper, uppercase variables denote the frequency-domain representation of their lowercase time-domain counterparts. The received signal at the LIS for the k-th subcarrier, $\mathbf{Y}(k)$, is given by

$$\mathbf{Y}(k) = \sum_{\mathrm{u}=1}^{\mathrm{U}} \mathbf{H}_u\,(k) S_u(k) + \mathbf{N}(k) \quad (1)$$

where $\mathbf{H}_u(k)$ represents the $N \times 1$ channel vector, between user u and the LIS, accounting for near-field propagation characteristics, via a deterministic Line-of-Sight (LoS) model with spherical wavefronts. The n-th element of $\mathrm{H}_u(k)$ is defined as

$$H_{u,n}(k) = \frac{\boldsymbol{\lambda}}{\mathbf{4\pi d_{u,n}}} \exp\left(\text{-j} \frac{2\pi}{\lambda} d_{\mathrm{u,n}} \right) \quad (2)$$

where $d_{u,n} = \sqrt{(x_u - x_n)^2 + (y_u - y_n)^2 + (z_u - z_n)^2}$ is the exact Euclidean distance between user u and the n-th LIS element. $\mathbf{N}(k)$ is the additive white Gaussian noise (AWGN) vector.

In summary, the proposed uplink system model is defined by U single-antenna users transmitting over K subcarriers to an LIS with N total elements. These elements are physically organized into P independent panels, where each panel contains N/P antenna elements. The resulting channel matrix $\mathbf{H}_k \in \mathbb{C}^{\mathbf{N}\times\mathbf{U}}$ and the received vector $\mathbf{Y}_k$ form the mathematical basis for the Partial LIS strategy (where only N_{act} elements are active) and the subsequent neural-network-based detection.

2.2. Partial LIS Selection

The LIS-based channel model assumes a near-field environment where spherical wavefronts are predominant, following the characterization established in [3,9]. This ensures that the distance-dependent phase shifts are accurately captured for each antenna element. Following the approach in [10], we apply selection matrix **A** to the surface, where $\mathbf{A} \in \{0,1\}^{Nact \times N}$ is a selection (indexing) matrix that extracts the active antenna elements from $\mathbf{Y}(k)$. We consider $N = P \times N_p$ where N stands for the total number of elements of the LIS, P the number of panels, and Np the number of antennas per panel.

Matrix **A** acts as a spatial filter that activates only a subset of panels $P_{active} \subset \{1, \ldots, P\}$, specifically those with the minimum distance to the target user. The reduced received vector $\mathbf{Y}_{part}(k) \in \mathbb{C}^{\mathbf{N_{act}} \times \mathbf{1}}$ becomes

$$\mathbf{Y}_{part}(k) = \mathbf{A}\mathbf{Y}(k) \tag{3}$$

where N_{act} denotes the number of selected antenna elements (rows of **A**). This equation significantly reduces the number of RF chains and the size of the signals to be processed by the digital front-end.

In the proposed Partial LIS framework, the selection logic ensures that only the panel with the shortest Euclidean distance to the user is activated. In this scenario, the number of active antennas is equal to the number of elements per panel ($N_{ant} = N_p$). For the simulated cases, N_{ant} is either 324 or 625. This represents a 75% reduction in active RF chains compared to the Full LIS baseline (where $\mathbf{A} = \mathbf{I}_N$), as we consider $P = 4$ panels. This significantly lowers the hardware complexity and power consumption without sacrificing the near-field focusing gain provided by the closest physical elements.

2.3. Characterization of Linear Receivers: MRC, EGC, ZF, and MMSE

After frequency-domain processing, the estimated symbol for a given user and subcarrier can be generally expressed as

$$\tilde{S}_u(k) = \mathbf{w}_u^H(k)\mathbf{Y}_p(k) \tag{4}$$

where $\mathbf{w}_u^H(k)$ represents the weight vector of the receiver. In this work, we consider four types of linear receivers:

1. Maximum Ratio Combining: The weights are simply the conjugate of the channel $\mathbf{w}_u(k) = \mathbf{H}_u(k)$, maximizing the Signal-to-Noise Ratio (SNR) but neglecting MUI.
2. Equal Gain Combining: Only the phase is corrected, using $\mathbf{w}_u(k) = exp\left(j \cdot arg\left(\mathbf{H}_u(k)\right)\right)$, which is hardware-friendly but offers lower performance.

For convenience, we define the selected (Partial LIS) channel matrix as $\mathbf{H}_p(k) \in \mathbb{C}^{N_{act} \times U}$, obtained by stacking the selected channel vectors of all users. Using the selection matrix **A** introduced in (3), this matrix can be written as $\mathbf{H}_p(k) = \mathbf{A}\mathbf{H}(k)$ where $\mathbf{H}(k) \in \mathbb{C}^{N \times U}$ is the full-aperture channel matrix.

In contrast, ZF and MMSE receivers process all users simultaneously to nullify or minimize MUI. The estimated symbols for all U users are given by

$$\tilde{S}(k) = \mathbf{W}^H(k)\mathbf{Y}_p(k) \tag{5}$$

where $\mathbf{W}^H(k)$ is a $U \times N_{act}$. Considering that $\mathbf{H}_p(k)$ is the selected channel matrix, the combining matrix is as follows:

1. Zero Forcing: Aims to nullify MUI by applying the pseudo-inverse of the channel matrix (which includes all $\mathbf{H}_u$ vectors): $\mathbf{W}^H(k) = \left(\mathbf{H}_p^H(k)\mathbf{H}_p(k)\right)^{-1}\mathbf{H}_p^H(\mathrm{k})$.
2. Minimum Mean Squared Error: Further improves ZF by considering the noise power: $\mathbf{W}^H(k) = \left(\mathbf{H}_p^H(k)\mathbf{H}_p(k) + \sigma^2 I\right)^{-1}\mathbf{H}_p^H(\mathrm{k})$.

It is important to note that while ZF and MMSE attempt to decouple all users by inverting the channel matrix, the low-complexity MRC and EGC receivers process each user independently. In near-field LIS scenarios with high user density, the spatial correlation between channel vectors $\mathrm{h}_u(k)$ increases, leading to a strong residual multi-user interference (MUI) component, as these linear combiners do not possess the capability to suppress inter-user contributions. This residual interference manifests as a performance floor, which limits the system's ability to improve the BER as the SNR increases, unless additional non-linear suppression, such as the proposed NN stage, is applied.

2.4. The Computational Complexity Bottleneck

While ZF and MMSE provide superior interference suppression, their practical implementation in LIS-assisted 6G systems is severely limited. Both require the calculation of a matrix inverse (or pseudo-inverse) for each frequency component (subcarrier k). In an SC-FDE (Single-Carrier Frequency-Domain Equalization) system with thousands of subcarriers and a high number of users (U), the complexity follows $O(U^3)$ per subcarrier. The choice of SC-FDE is particularly suitable for LIS-based 6G systems due to its low Peak-to-Average Power Ratio (PAPR). Unlike OFDM (Orthogonal Frequency Division Multiplexing), SC-FDE maintains a constant envelope-like signal, allowing the use of high-efficiency power amplifiers at the user terminal. This is critical in LIS environments where massive connectivity and energy-constrained devices are expected. Furthermore, SC-FDE shifts the equalization complexity to the receiver side (the LIS controller), where the proposed deep learning-based detection can then be applied in the frequency domain to suppress multi-user interference with high efficiency.

ZF and MMSE are not only extremely demanding in terms of processing power but also highly energy-inefficient, contradicting the green communication goals of 6G. This bottleneck motivates the use of low-complexity $\mathbf{w}_u(k)$ vectors based on MRC or EGC receivers, combined with the intelligent, non-linear interference suppression proposed in the following section.

3. Proposed NN-Based Partial LIS Architecture

This section details the proposed hybrid framework, which integrates the spatial efficiency of the Partial LIS concept with the advanced detection capabilities of NNs. The goal is to circumvent the $O(U^3)$ complexity bottleneck previously identified, while maintaining high spectral efficiency. The shift from traditional iterative detection to a learning-based approach is motivated by the ability of NNs to approximate complex non-linear mappings without the overhead of matrix inversions [21].

3.1. Synergy Between Selective Aperture and Learning-Based Detection

The transition from traditional linear processing to the proposed learning-based architecture follows a compensatory logic. Linear receivers, such as MRC and EGC, are computationally efficient but suffer from an inability to distinguish between the desired signal and the non-linear interference patterns typical of reduced-aperture LIS. In this context, the neural network is introduced not as a replacement for the entire reception chain, but as a non-linear refinement stage. It operates on the output of the linear combiner, treating the residual multi-user interference (MUI) and the distortions caused by panel correlation as structured noise patterns. The network performs a non-linear symbol-by-symbol estimation to compensate for these residual distortions and noise after the linear combining stage. This hybrid approach allows the system to maintain the low-latency benefits of linear combining while achieving the detection accuracy of high-complexity iterative receivers.

https://doi.org/10.3390/app16073429

The proposed architecture operates on a dual-stage optimization principle. First, at the hardware level, the Partial LIS mechanism reduces the number of active RF chains by selecting only the panels in the vicinity of the user. Second, at the digital processing level, a neural network replaces the traditional matrix inversion required for high-performance detection.

In practical deployments, the activation of the closest panels to the user is determined during the initial channel-sounding phase. The central controller then applies a threshold-based selection or simply identifies the N_{sub} panels with the highest energy profiles. This ensures that only the panels within the user's 'spatial footprint' are activated, minimizing power consumption while capturing the majority of the channel's energy.

The signal received from the u-th user, after the initial linear combining stage, can be mathematically expressed as

$$\tilde{S}_u(k) = \mathbf{w}_\mathrm{u}^\mathrm{H}\mathbf{H}_{u,p}(k)S_u(k) + \mathbf{w}_u^H(k)\sum_{j\neq u}^{U} \mathbf{H}_{\mathrm{j,p}}(k)S_{\mathrm{j}}(k) + \mathbf{w}_u^H(k)\mathbf{N}_\mathrm{p}(k) \tag{6}$$

where $\mathbf{w}_\mathrm{u}^\mathrm{H}$ denotes the Hermitian transpose of the weight vector for the u-th user, corresponding to the linear combining stage (MRC or EGC). Moreover, $j \in \{1,\ldots,U\}, j \neq u$. The first term of (6) represents the desired signal, the third term is the processed noise, and the middle summation represents the MUI. In Partial LIS environments, the reduced spatial resolution often leads to non-orthogonal channel vectors $\mathbf{h}_u$ and $\mathbf{h}_j$, significantly increasing the magnitude of this interference term. The proposed MLP is specifically designed to perform a non-linear symbol-by-symbol estimation. By learning the distortion patterns caused by the residual MUI and noise, the MLP maps the corrupted linear estimates back to the original QPSK constellation points.

As detailed in Table 1, the proposed MLP architecture consists of an input layer with two neurons (processing the I and Q components of each symbol), followed by two hidden layers (L = 2) and an output layer. The first hidden layer comprises 20 neurons, while the second comprises 10. The ReLU activation function is employed in both hidden layers to learn complex MUI patterns while maintaining a low computational footprint compared to transcendental functions. To ensure maximum throughput and minimum processing latency, normalization layers were omitted.

Table 1. Proposed MLP architecture specifications.

Layer	Type	Neurons	Activation
Input	Fully Connected	2 (I/Q)	-
Hidden 1	Fully Connected	20	ReLU
Hidden 2	Fully Connected	10	ReLU
Output	Fully Connected	2 (I/Q)	Linear

The synergy lies in the fact that the NN is specifically trained to recognize the interference patterns produced by the reduced aperture of the Partial LIS and by the linear combining stage (MRC/EGC). This design choice aligns with recent trends where deep learning is employed to optimize physical layer parameters, such as antenna selection in MIMO systems [10] and beamforming refinement in near-field LIS environments [19]. By leveraging these learning capabilities, as explored in TeraHertz hybrid architectures [17], our system avoids energy-intensive matrix inversions. While the selection of N_p panels in Section 2.2 significantly lowers energy consumption, it also results in a higher correlation between the channel vectors $\mathbf{H}_u\,(k)$. The NN-based receiver is designed to handle these non-linearities and residual MUI more effectively than simple linear combiners.

The generalization capability of the proposed receiver is a key design feature. By employing a diverse training set that covers the entire near-field region, the NN learns to suppress interference patterns that are characteristic of the Partial LIS geometry. This architecture follows the principles established in previous research [14], where a similar deep learning approach demonstrated significant robustness and generalization in Full LIS architectures. In this study, we confirm that these properties are preserved when transitioning to a Partial LIS framework. The network effectively adapts to the residual MUI resulting from the independent processing of antenna panels, maintaining consistent performance even when the user terminal experiences moderate spatial shifts or when the panel selection is updated dynamically.

3.2. Non-Linear Interference Suppression Stage

To address the limitations of linear receivers, we propose a specialized MLP network. Similar approaches combining neural networks with equalization stages have shown significant potential in improving signal detection in complex wireless environments [22].

Following the initial processing, the signals are combined using low-complexity techniques. For the MRC-based stage, the estimated signal for the u-th user at the k-th subcarrier is obtained through the weight vector $\mathbf{W}_u\ (k) = \mathbf{H}_u\ (k)$:

$$\tilde{S}_u(k) = \mathbf{H}_u^H(k)\mathbf{Y}_p(k) \tag{7}$$

As previously established, $\tilde{S}_u(k)$ is corrupted by MUI generated in the linear combining stage of MRC (or EGC). To suppress this without resorting to the pseudo-inverse calculations of ZF/MMSE, $\tilde{S}_u(k)$ is fed into a neural network. The NN architecture, illustrated in Figure 1, is an MLP designed to approximate the non-linear suppression function

$$\hat{S}_u(k) = f_{MLP}\left(\mathbf{X}_{input,u}(k); \theta\right) \tag{8}$$

where θ represents the weights and biases optimized during training (a training sequence can be employed). The MLP was trained using the Adam optimizer with the specific hyperparameters summarized in the Section 4.

The choice of this hybrid architecture, where the NN acts as a post-processor, is strategically designed to handle the high dimensionality of the LIS. Bypassing the linear combiner to map the received vector $\mathbf{y}_p(k)$ directly to the symbols would result in an exceedingly large input layer, proportional to the high number of antenna elements (N_{ant}). Such an end-to-end model would face significant training challenges due to the vast search space and parameter variability. By employing MRC/EGC as a pre-processing stage (see Figure 1), the system performs a crucial dimensionality reduction, narrowing the input from the high-dimensional LIS space to a single complex-valued estimate per user. As seen in Figure 1, the NN processes each user's stream independently, focusing on a simplified I/Q mapping that ensures a more stable training process and lower latency. This allows the NN to focus on a simplified set of variables, ensuring a more stable training process and a computationally efficient inference stage.

It is important to contrast the proposed one-shot MLP with the iterative NN architecture described in [14]. In Full LIS environments, iterative processing is often used to refine detection; however, the Partial LIS profile introduces higher spatial correlation and wider interference beams due to the reduced active aperture. We found that a specialized one-shot mapping is more effective at capturing these specific non-linear patterns in a single pass. This not only addresses the increased MUI of partial surfaces but also significantly reduces processing latency, making the receiver more suitable for real-time 6G applications compared to the multi-pass iterative approach.

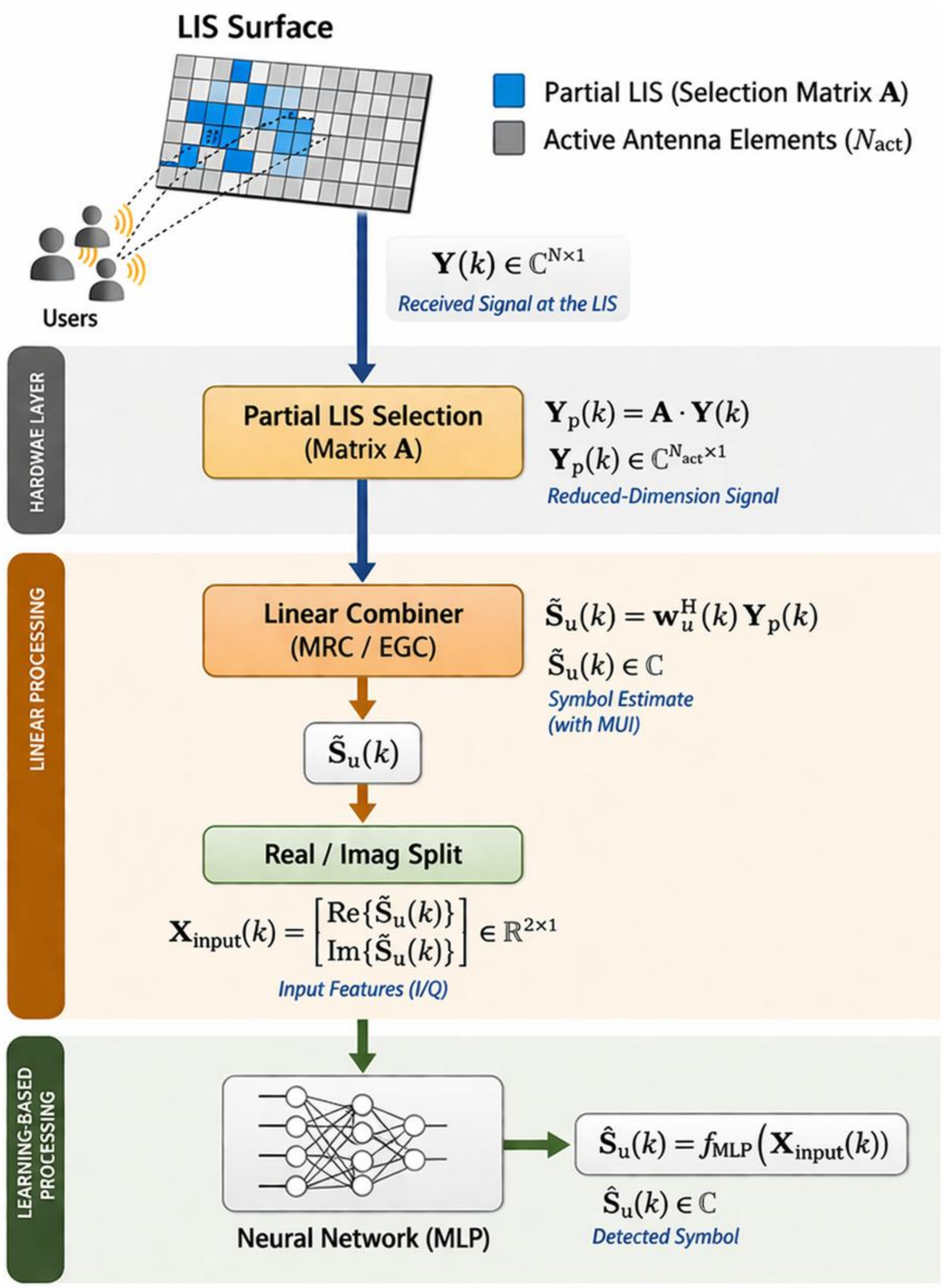

Figure 1. Proposed hybrid receiver architecture.

As can be seen in Figure 1, the proposed MLP architecture processes complex-valued signals by splitting them into real and imaginary components at the input layer, $\mathbf{X}_{\text{input}}(k) = \left[\Re\left\{\tilde{S}_u(k)\right\}, \Im\left\{\tilde{S}_u(k)\right\}\right]^{\mathbf{T}}(k)$; the network consists of two hidden layers ($H_1 = 20$, $H_2 = 10$ neurons) utilizing Rectified Linear Unit (ReLU) activations to compensate for the non-linear shifts in the constellation caused by the reduced active aperture (N_{act}) and the resulting residual MUI. Training is performed offline using the Adam optimizer and Mean Squared Error (MSE) loss over a dataset of channel realizations specifically reflecting the Partial LIS environment. Unlike general-purpose models, this specialized training enables the network to compensate for the higher spatial correlation and unique interference profiles resulting from the reduced active aperture (N_{sub}).

3.3. Computational Efficiency Analysis

The proposed architecture provides a significant reduction in computational complexity compared to the benchmarks discussed in Section 2.3 (ZF/MMSE), substantiated by the following analysis:

1. Avoidance of Matrix Inversion: To quantify this advantage, a matrix inversion for U = 4 users requires on the order of 128 floating-point operations (FLOPs), but this cost scales cubically approximately to 1024 FLOPs when U = 8. In a massive MIMO/LIS context with N = 1024 antennas, the total ZF processing (including matrix multiplication) can exceed 16,000 FLOPs per subcarrier for U = 8, whereas our proposed MLP keeps a constant and much lower overhead of 520 FLOPs. This reduces the per-symbol detection complexity to a linear scale, $O(N_{partial})$.
2. Aperture Reduction (Partial LIS): By utilizing the selection matrix **A**, the system only processes antenna elements instead of the total N_{total} elements of the Full LIS. Since $N_{partial} << N_{total}$ (e.g., a 75% reduction in active elements), the number of floating-point operations (FLOPs) in the linear combining stage scales down proportionally.
3. Inference Efficiency (NN Overhead): The FLOP count for the NN inference is derived as $2 \times (I \cdot H_1 + H_1 \cdot H_2 + H_2 \cdot O)$ where I = 2, H_1 = 20, H_2 = 10, and O = 2 represent the neurons per layer. This results in 520 FLOPs per detected symbol. In contrast, the linear combining stage for a Partial LIS with $N_{partial}$ elements requires $4N_{partial} - 2$ FLOPs. For a scenario with $N_{total} = 1024$ and a 75% reduction $N_{partial} = 256$), the total complexity drops from approximately 4094 FLOPs (Full LIS) to 1542 FLOPs (Proposed), representing a net saving of ~62%, even including the NN overhead.
4. Quantitative Comparison: As summarized in Table 2, while the Full LIS complexity is dominated by $O(N_{total})$, the proposed Partial LIS with NN suppression scales with $O(N_{partial}) + C$. This results in a net reduction in computational requirements, enabling real-time 6G implementation with lower power consumption.

Table 2. Computational complexity comparison between traditional linear receivers and the proposed deep learning-based Partial LIS architecture.

Receiver Type	**Complexity Order**	**Scaling Factor**	**Main Operations**
ZF/MMSE	$O(U^3 + N_{total})$	High (Matrix Inversion)	Inversion + Combining
Full LIS (MRC/EGC)	$O(N_{total})$	Linear (High N)	Combining (All Elements)
Iterative Partial LIS + Iterative MRC/EGC	$O(I_{iter} + N_{partial})$	Moderate	Multiple Processing Passes
Proposed Partial LIS + NN	$O(N_{partial}) + C$	Lowest (Low N)	Combining (Subset) + MLP

As illustrated in Table 2, the proposed architecture offers a clear advantage over the iterative MRC/EGC baseline [10]. While iterative methods require multiple passes over the high-dimensional antenna data (I_{iter}) to refine the signal, the proposed NN-based receiver operates in a one-shot fashion. By replacing the iterative process with a shallow MLP, the computational burden is transformed from a multiple of the aperture dimension to a single combining stage plus a small constant overhead (C). This results in lower processing latency and a net reduction in FLOPs, as the fixed cost of the NN inference is significantly lower than the cost of repeated large-scale linear combining.

4. Simulation Results and Performance Analysis

In this section, we provide a comprehensive performance evaluation of the proposed hybrid architecture through Monte Carlo simulations. The performance is evaluated in terms of BER versus the energy per bit to noise power spectral density ratio ($^{E_b}/_{N_0}$).

The primary objective is to assess the efficiency of integrating the selective panel mechanism with NN-based detection in a multi-user uplink scenario. By comparing the proposed scheme with traditional linear benchmarks, we aim to validate its robustness against the increased spatial correlation, interference inherent in reduced-aperture LIS configurations, and residual MUI generated in the decoding process of low-complexity linear receivers (MRC/EGC). It is important to emphasize that the terms '324 elements' and '625 elements' refer to the antenna density per individual panel (N_{ant}). Consequently, in the Full LIS architecture, the receiver processes a total of $4 \times N_{ant}$ signals. In contrast, the proposed Partial LIS framework selectively processes only N_{ant} signals (either 324 or 625), achieving a 75% reduction in RF chain complexity while maintaining high detection performance through the NN stage.

4.1. Simulation Setup and Metrics

The evaluation is conducted within an SC-FDE framework, assuming Quadrature Phase Shift Keying (QPSK) modulation and a near-field propagation environment, as described in Section 2. The LIS is composed of a massive array of elements, from which a subset of panels is dynamically selected for each user.

To provide a rigorous evaluation of the proposed deep learning-based receiver, the datasets were generated using Monte Carlo simulations based on the system model described in Section 2. A total of 10^5 independent channel realizations were produced, encompassing different user positions and near-field fading conditions. This dataset was partitioned into three subsets: 70% for the training phase, 15% for validation (used for hyperparameter tuning and early stopping), and the remaining 15% for final performance testing.

As summarized in Table 3, the training phase was executed using the Adam optimizer with a Mean Squared Error (MSE) loss function, a batch size of 1024, and a fixed learning rate of 0.001. To ensure the model's reliability and prevent overfitting, the process included a validation-based early stopping criterion, which was triggered if the validation loss failed to decrease for a patience period of 100 epochs. Furthermore, overfitting was strictly monitored by analyzing the convergence of training and validation loss curves; the final model was selected at the point where the validation loss reached its minimum. The results presented hereafter reflect the average performance over thousands of independent channel blocks, highlighting the trade-offs between hardware simplification (panel selection) and signal processing intelligence (learning-based suppression).

Table 3. Neural network training and simulation parameters.

Simulation Method	Monte Carlo (10^5 trials per point)
Noise Model	AWGN (additive white Gaussian noise)
Channel Model	Near-field LoS (spherical wavefronts)
Power Control	Perfect
Network Architecture	Multi-Layer Perceptron
Number of Hidden Layers	2
Neurons per Hidden Layer	20 (1st layer), 10 (2nd layer)
Activation Functions	ReLU (hidden layers), Linear (output layer)
Training Dataset Size	10^6
Data Split	70% Training/15% Validation/15% Testing

https://doi.org/10.3390/app16073429

Initial Learning Rate	10^{-3}
Learning Rate Scheduler	None
Optimizer	Adam
Loss Function	Mean Squared Error
Learning Rate	0.001
Number of Epochs	100
Batch Size	1024
Maximum Epochs	500 (with early stopping)
Overfitting Monitoring	Validation Loss Tracking
Stopping Criteria	Early Stopping (patience = 20 epochs)

The total aperture of the four-panel LIS is approximately 0.63×0.63 m. At the reference frequency of 28 GHz, the Rayleigh distance $d_R = {2D^2}/{\lambda}$ is significantly larger than the maximum user distance of 10 m. Specifically, with $D \approx 0.89$ m (diagonal of the total aperture), d_R extends to approximately 148 m. This ensures that the entire user ensemble (located between 2 m and 10 m) is strictly positioned within the Fresnel region, where spherical wavefront modeling is essential.

4.2. Performance Comparison: Full LIS vs. Partial LIS

This subsection establishes a baseline for our study by examining the performance trade-offs between a Full LIS architecture and the proposed Partial LIS framework. In the Full LIS setup, the entire surface remains active, whereas the Partial LIS approach restricts signal processing to specific panels. To clearly isolate the effects of reduced physical aperture, we focus here on the performance of standard linear low-complexity combiners, specifically MRC and EGC, before any neural-network-based suppression is applied.

Figure 2 presents the BER results for a load environment of $U = 8$ users, comparing antenna densities of $N_{\text{ant}} = 324$ and $N_{\text{ant}} = 625$ per panel (four panels and one panel [Partial LIS] are considered). The LIS is composed of four independent panels arranged in a 2×2 grid. Each panel is a UPA with ${\lambda}/{2}$ spacing between elements. The distance between panel centers (D_c) is determined by the panel size $N \times {\lambda}/{2}$), resulting in a compact aperture designed for near-field operation at, e.g., 28 GHz. For the 625-element case, D_c is approximately 0.5 m, ensuring the system captures distinct spatial signatures from each panel.

As observed, the Partial LIS architecture inherently suffers a performance penalty when compared to the Full LIS baseline due to the reduced active aperture and lower spatial resolution. However, the proposed NN stage effectively suppresses this loss, as shown in Figure 2, by recovering the signal integrity and bringing the performance close to the Full LIS linear benchmarks.

A noteworthy observation arises when analyzing the performance in low-to-moderate SNR regimes, specifically up to approximately 12 dB, where the Partial LIS configuration achieves superior BER results compared to the Full LIS architecture. This phenomenon is primarily justified by the reduction in MUI levels and the noise accumulated during the combining process. Although the Full LIS captures a greater amount of total signal energy, it also collects a disproportionate amount of interference from distant users that, due to their geometry, possess a diminished capacity to effectively isolate the desired signal. By selectively activating only the panels closest to each user, the Partial LIS functions as an inherent spatial filter that discards these highly noisy and interfered components, resulting in an improved signal-to-interference-plus-noise ratio in scenarios where signal power is still limited.

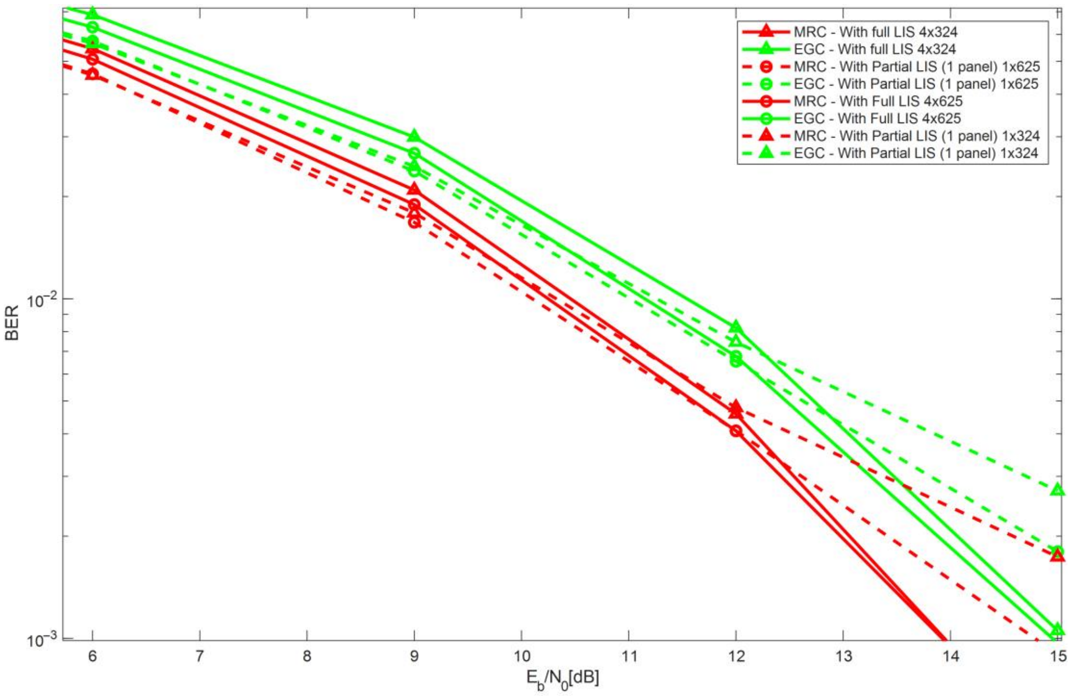

Figure 2. Average BER performance comparison between Full LIS and Partial LIS architectures for $U = 8$ users, considering antenna densities of $N_{ant} = 324$ and $N_{ant} = 625$ per panel with MRC and EGC receivers (iterative receivers).

As the SNR increases beyond the 12 dB threshold, the curves reveal that the diminished physical aperture eventually limits the surface's ability to perform precise near-field spatial focusing. This limitation, inherent to the reduced-aperture operation, creates a wider spatial beam that contributes to a performance noise floor at elevated E_b/N_0 values. Furthermore, the results show that MRC consistently outperforms EGC across the entire range. This is justified by the fact that MRC performs an optimal ratio combining by considering both the phase and the amplitude of the channel, whereas EGC only aligns the signal phases. Consequently, the residual MUI generated during the decoding process is more pronounced in EGC, leading to a higher saturation level (noise floor) compared to MRC. Reducing the antenna density to 324 elements further exacerbates these effects, underscoring that a learning-based suppression stage is essential to overcome the noise floor generated by both the receiver's simplified architecture (and its residual MUI generated in the decoding process) and the reduced-aperture constraints, particularly in the high-SNR regime.

4.3. Impact of NN-Based Recovery and Antenna Density

Following the baseline characterization of the Partial LIS framework, this subsection evaluates the capacity of the proposed NN-based stage to recover link quality and suppress residual interference. The analysis specifically explores the synergy between low-complexity linear iterative combiners (MRC/EGC) and the MLP-based suppressor, focusing on how this hybrid approach performs under different antenna densities per panel, namely 625 and 324 elements.

As illustrated in Figure 3, the integration of the NN stage produces a substantial and consistent improvement in BER performance across all tested configurations. While the conventional iterative receivers (dashed lines) reach an interference-limited noise floor at high SNR, the NN-enhanced versions maintain a robust descent. This trend confirms that the MLP is highly effective at identifying and strongly suppressing the residual MUI generated during the decoding process of MRC/EGC combiners, as well as the residual interference resulting from the reduced-aperture LIS configuration. By learning these complex non-linear patterns, the NN effectively removes the noise floor that traditional iterative methods, previously explored in [10], fail to resolve.

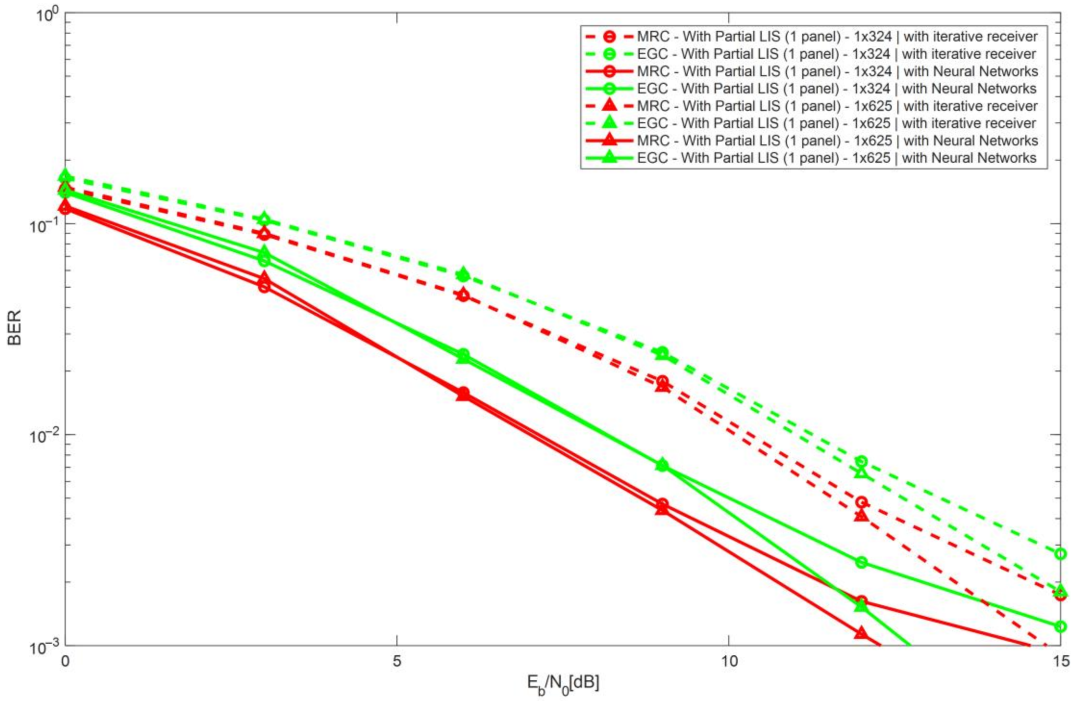

Figure 3. Average BER performance considering antenna densities of $N_{ant} = 324$ and $N_{ant} = 625$ for Partial LIS, comparing iterative and NN receiver for MRC and EGC.

A particularly compelling result observed in these simulations is the trade-off between physical hardware and computational intelligence. It is noteworthy that the MRC + NN configuration utilizing only 324 antennas achieves a performance level that tends to surpass the iterative MRC receiver with 625 antennas. This finding is central to our study, as it proves that a well-trained, low-complexity neural network can effectively compensate for a nearly 50% reduction in the physical antenna elements of the surface. By shifting the processing burden from the power-intensive RF front-end to a streamlined digital learning stage, the system maintains high-quality communication while significantly decreasing the overall energy footprint and hardware complexity.

4.4. System Scalability and User Loading

Beyond the impact of antenna density, it is critical to evaluate the robustness of the proposed architecture when subjected to increased user loads. This subsection examines the scalability of the Partial LIS framework by comparing the system performance under a low-load scenario, with $U = 4$ users, against a high-load scenario involving $U = 8$ users. For this analysis, we maintain a fixed density of 625 antennas per panel to isolate the effects of MUI on the recovery capability of the MLP-based receiver.

The results depicted in Figure 4 demonstrate that as the number of active users doubles, the conventional iterative receivers suffer from significant performance degradation. This is evidenced by a substantial rightward shift in the BER curves and the emergence of a much higher interference floor, which reflects the increased difficulty in spatially separating user signals as the density of the transmissions grows. Under these stressed conditions, the traditional linear combining and iterative stages struggle to maintain reliable communication. The increased user load significantly elevates the noise floor generated during the decoding process, which, coupled with the spatial limitations of the partial aperture, creates a severe performance bottleneck for classical receivers.

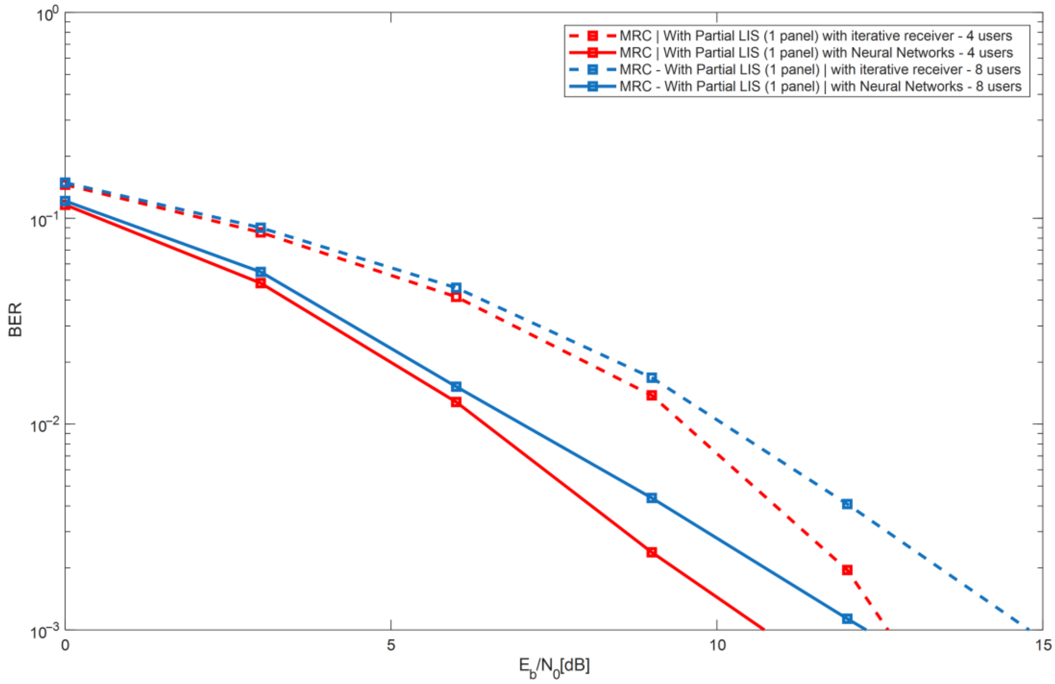

Figure 4. BER performance of the proposed one-shot NN-based MUI suppression stage compared to traditional linear receivers (MRC) for $N_{ant} = 625$, for $U = 4$ versus $U = 8$ users.

In contrast, the NN-enhanced receiver displays remarkable resilience to the increase in user load. While a performance gap between the $U = 4$ and $U = 8$ scenarios is expected due to the physical limits of the channel, the MLP-based suppression stage narrows this gap compared to its iterative counterparts. The non-linear learning stage effectively adapts to the more complex interference environment of the eight-user case, achieving a BER level that remains closer to the low-load baseline. This stability underscores the scalability of the proposed synergistic approach, proving that the integration of neural networks allows the Partial LIS architecture to handle dense connectivity requirements in 6G environments without requiring a proportional increase in hardware complexity or active antenna elements.

4.5. Proposed Hybrid Solution vs. High-Complexity Benchmarks

The final stage of our performance analysis involves validating the proposed hybrid framework against established high-complexity benchmarks, specifically the ZF and MMSE receivers. While these traditional algorithms are known for their optimal or near-optimal interference suppression capabilities in Full LIS environments, they impose a prohibitive computational burden due to the requirement for large-scale matrix inversions, whose requirements increase with the increase in the number of antennas. This subsection demonstrates how the synergistic combination of Partial LIS and MLP-based suppression achieves competitive results with a significantly lower processing overhead.

As illustrated in Figure 5, a critical observation is that both the Full LIS and Partial LIS NN-enhanced receivers consistently outperform the ZF/MMSE benchmarks across the entire SNR range. These results specifically highlight the impact of antenna resolution on system performance. It is possible to observe that even for a scenario with a high number of users ($U = 24$), the performance of the NN with Partial LIS remains close to the established benchmarks, confirming its robustness and ability to scale with antenna density.

https://doi.org/10.3390/app16073429

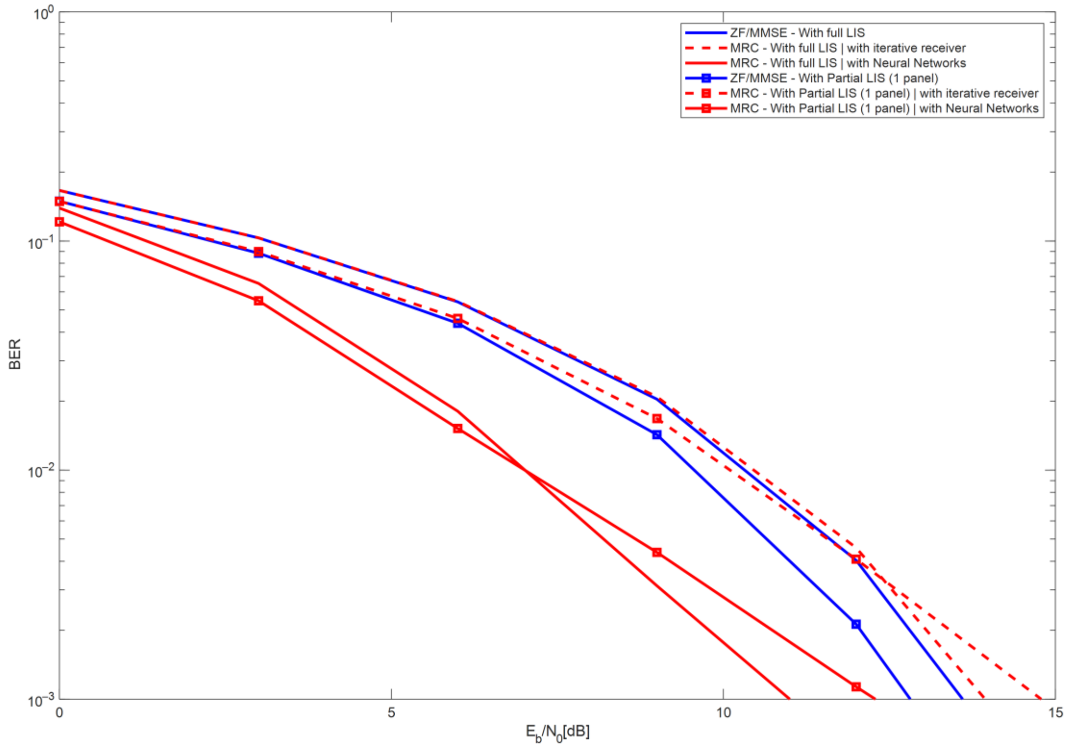

Figure 5. Impact of Partial LIS vs. Full LIS on the BER performance of the NN-aided versus iterative receiver (MRC) and ZF/MMSE, for $U = 24$ users.

A noteworthy observation is the overlap between the ZF and MMSE curves. This occurs because, under the simulated deterministic Line-of-Sight (LoS) near-field conditions and the considered SNR range, the noise power becomes negligible compared to the signal power. Consequently, the MMSE weight matrix converges to the ZF pseudo-inverse, leading to identical BER performance. This explains why the high-complexity benchmarks appear as a single curve, providing a reference for the maximum interference suppression theoretically possible through linear matrix inversion in this environment. While ZF and MMSE provide optimal linear decoupling under ideal conditions, they are inherently constrained by their inability to compensate for non-linear distortions and complex spatial correlations. This performance gap is one key motivation for the neural-network-based stage.

The superiority of the NN-aided approach over classical ZF and MMSE receivers stems from the fundamental difference between linear processing and non-linear mapping. ZF and MMSE rely on the inversion of the channel matrix, which is an optimal strategy only when the interference is strictly linear and the channel state information is perfect. However, in Partial LIS deployments, the reduced aperture creates complex spatial correlation and residual multi-user interference (MUI) that exhibit non-linear characteristics. The MLP, through its non-linear activation functions (ReLU), is capable of learning these intricate interference signatures and the specific noise floor induced by the simplified MRC/EGC stages. Consequently, the NN acts as a specialized non-linear filter that corrects distortions that are mathematically 'invisible' to the linear operations of ZF and MMSE.

This demonstrates that the non-linear processing capability of the MLP is superior at suppressing both the MUI and the residual interference that linear receivers (MRC/EGC) fail to suppress. As described, ZF and MMSE curves overlap due to the high SNR convergence. However, in this high-load scenario ($U = 24$), the performance gap between MRC and EGC is further widened, as the phase-only limitation of EGC makes the multi-user suppression task significantly more challenging.

Most notably, the results reveal an unconventional crossover behavior: at low SNR levels (up to approximately 7 dB), the Partial LIS NN configuration achieves better BER results than its Full LIS NN counterpart. This crossover is physically explained by the noise accumulation effect: At low SNR, the contribution of distant panels in the Full LIS setup is outweighed by the additional thermal noise and MUI they capture. By contrast, the Partial LIS focuses only on the high-SNR signal components closest to the user (spatial footprint), providing a higher-quality feature set that allows the NN to perform more effective MUI suppression.

Beyond this threshold, although the Full LIS NN setup regains its spatial diversity advantage, the proposed Partial LIS hybrid framework continues to significantly surpass the performance of classical ZF/MMSE. This validates the core thesis of our work, positioning the MLP-based Partial LIS as a highly efficient and 'green' solution. Furthermore, the MLP inference consists of feed-forward matrix operations that can be massively parallelized in hardware (e.g., FPGAs or ASICs), resulting in the deterministic low latency required for URLLC.

Furthermore, while this work compares the proposed hybrid framework against exact ZF and MMSE implementations, it is important to acknowledge the existence of low-complexity linear detection approximations, such as those based on Neumann series or Chebyshev iterations. A comprehensive 'green' assessment comparing the MLP-based approach with these iterative linear approximations is envisioned as future work to further benchmark the energy efficiency of neural-network-aided receivers.

Despite these advantages, the proposed solution has some limitations that merit further discussion. First, the efficiency of the MLP depends on the alignment between offline training and real-time conditions. In scenarios with significant user mobility or channel aging, performance may degrade. To address this, we envision an online adaptation strategy where the NN undergoes periodic incremental retraining (fine-tuning). Given the lightweight MLP architecture, this process can be performed using a small buffer of recently received pilot symbols. By updating only the weights of the final layers, the computational overhead remains minimal. Furthermore, the use of transfer learning allows a pre-trained base model to quickly adapt to a specific user's trajectory, ensuring that the signaling overhead does not compromise spectral efficiency.

5. Conclusions

This article proposed and evaluated a deep learning-based receiver architecture for 6G uplink scenarios, integrating the spatial selectivity of Partial LIS with the advanced detection capabilities of NN-based interference suppression. By activating only the antenna panels closest to the user terminal, the proposed system significantly reduces the hardware footprint and the power consumption of the RF front-end. The inherent performance loss increased due to MUI caused by this reduced aperture and the residual MUI generated by the independent processing of low-complexity combiners were effectively suppressed by a specialized MLP-based stage. This NN approach replaces the complexity of traditional matrix-inversion receivers by efficiently removing the performance noise floor that typically limits the effectiveness of linear combining in these scenarios.

The simulation results provided several critical insights into future 6G deployments. First, the Partial LIS architecture demonstrated a noise reduction effect at lower SNR regimes (up to 7–12 dB). This occurs because, in a Full LIS configuration, the receiver sums noise components from all elements across the entire surface. However, in the near-field scenario, a specific user's energy is concentrated in a limited spatial footprint. By activating only the panels within this footprint (Partial LIS), the system effectively improves the

SNR by excluding noise from inactive areas where the user's signal power is negligible. This spatial selection acts as a hardware-level noise-gating mechanism, allowing the Partial LIS to outperform the Full LIS when the channel is noise-limited. Second, the integration of the NN-based stage proved to be superior to traditional matrix-inversion-based methods like ZF and MMSE in terms of the complexity–performance trade-off. Notably, the neural-network-enabled receiver was able to bridge the performance gap between different antenna densities, showing that a 625-antenna setup with NN enhancement can exceed the performance of more complex iterative receivers while maintaining a lower computational footprint.

The most pivotal finding of this research is that computational intelligence can effectively substitute for physical hardware density. The proposed MRC-NN hybrid solution in a Partial LIS configuration not only demonstrated remarkable resilience to increased user loads but also surpassed the performance of Full LIS benchmarks using traditional linear processing. This confirms that the synergy between spatial panel selection and nonlinear learning provides a scalable, energy-efficient, and "green" solution for 6G networks. Future research will explore the adaptation of this framework to dynamic multiuser mobility and the optimization of the MLP architecture for real-time hardware implementation on Field-Programmable Gate Array (FPGA) platforms.

Author Contributions: Methodology, M.M.d.S.; Validation, M.M.d.S.; Investigation, H.O. and R.D. All authors contributed equally to the article. All authors have read and agreed to the published version of the manuscript.

Funding: This work was funded by national funds through FCT—Fundação para a Ciência e a Tecnologia—as part the Project C2I2/UAL—Refª UID/05567/2025—https://doi.org/10.54499/UID/05567/2025. Moreover, this work was partially funded by national funds through FCT—Fundação para a Ciência e a Tecnologia, I.P., and, when eligible, co-funded by EU funds under project/support UID/50008/2025—c, with DOI identifier https://doi.org/10.54499/UID/50008/2025.

Institutional Review Board Statement: Not applicable.

Informed Consent Statement: Not applicable.

Data Availability Statement: The data were obtained using Monte Carlo simulations and implemented using MATLAB R2024b. The original contributions presented in this study are included in the article. Further inquiries can be directed to the corresponding author.

Acknowledgments: We acknowledge the support of FCT/MCTES, as described above in "Funding". We also acknowledge the support of Autonoma TechLab for providing an interesting environment to carry out this research.

Conflicts of Interest: The authors declare no conflicts of interest.

References

1. ITU-R. Framework and Target Objectives of the Future Development of IMT for 2030 and Beyond. In *Recommendation ITU-R M.2160-0*; ITU: Geneva, Switzerland, 2023.
2. Hu, S.; Rusek, F.; Edfors, O. Beyond Massive MIMO: The Potential of Data Transmission with Large Intelligent Surfaces. *IEEE Trans. Signal Process.* **2018**, *66*, 2746–2758. https://doi.org/10.1109/tsp.2018.2816577.
3. Decarli, N.; Dardari, D. Communication Modes with Large Intelligent Surfaces in the Near Field. *IEEE Access* **2021**, *9*, 165648–165666. https://doi.org/10.1109/access.2021.3133707.
4. Huang, C.; Hu, S.; Alexandropoulos, G.C.; Zappone, A.; Yuen, C.; Zhang, R.; Di Renzo, M.; Debbah, M. Holographic MIMO Surfaces for 6G Wireless Networks: Opportunities, Challenges, and Trends. *IEEE Wirel. Commun.* **2020**, *27*, 118–125. https://doi.org/10.1109/mwc.001.1900534.

5. Bjornson, E.; Sanguinetti, L. Rayleigh fading modeling and channel hardening for reconfigurable intelligent surfaces. *IEEE Wirel. Commun. Lett.* **2020**, *10*, 830–834. https://doi.org/10.1109/lwc.2020.3046107.
6. Di Renzo, M.; Debbah, M.; Phan-Huy, D.-T.; Zappone, A.; Alouini, M.-S.; Yuen, C.; Sciancalepore, V.; Alexandropoulos, G.C.; Hoydis, J.; Gacanin, H.; et al. Smart radio environments empowered by reconfigurable AI meta-surfaces: An idea whose time has come. *EURASIP J. Wirel. Commun. Netw.* **2019**, *2019*, 129. https://doi.org/10.1186/s13638-019-1438-9.
7. Mu, X.; Xu, J.; Liu, Y.; Hanzo, L. RIS-Aided Near-field Communications for 6G: Opportunities and Challenges. *arXiv* **2023**, arXiv:2312.13004.
8. Felizardo, K.B.; Arboleda, E.R. Next-generation antennas key enabler: Intelligent Reflecting Surfaces (IRS) technology potential to address limitations of traditional antennas. *Int. J. Sci. Res. Arch.* **2024**, *12*, 2608–2613. https://doi.org/10.30574/ijsra.2024.12.1.1136.
9. Bjornson, E.; Özlem, T.; Sanguinetti, L. A primer on near-field beamforming for arrays and reconfigurable intelligent surfaces. In Proceedings of the 2021 55th Asilomar Conference on Signals, Systems, and Computers (ACSSC), Pacific Grove, CA, USA, 31 October–3 November 2021; pp. 105–112.
10. Marques da Silva, M.; Gashtasbi, A.; Dinis, R.; Pembele, G.; Correia, A.; Guerreiro, J. On the Performance of Partial LIS for 6G Systems. *Electronics* **2024**, *13*, 1035. https://doi.org/10.3390/electronics13061035.
11. Falconer, D.; Ariyavisitakul, S.; Benyamin-Seeyar, A.; Eidson, B. Frequency domain equalization for single-carrier broadband wireless systems. *IEEE Commun. Mag.* **2002**, *40*, 58–66. https://doi.org/10.1109/35.995852.
12. Borges, D.; Montezuma, P.; Dinis, R. Low complexity MRC and EGC based receivers for SC-FDE modulations with massive MIMO schemes. In *2016 IEEE Global Conference on Signal and Information Processing (GlobalSIP), Washington, DC, USA, 7–9 December 2016*; IEEE: Piscataway, NJ, USA, 2016; pp. 675–678. https://doi.org/10.1109/GlobalSIP.2016.7905927.
13. Torres, P.; Charrua, L.; Gusmao, A. On the Uplink Detection Performance in MU-MIMO Broadband Systems with a Large Number of BS Antennas. In Proceedings of the 18th International OFDM Workshop 2014, Essen, Germany, 27–28 August 2014.
14. Marques da Silva, M.; Pembele, G.; Dinis, R. Neural-Network-Based Interference Cancellation for MRC and EGC Receivers in Large Intelligent Surfaces for 6G. *Electronics* **2025**, *14*, 2083. https://doi.org/10.3390/electronics14102083.
15. Lv, X.; Zhang, X.; Gao, H.; He, T.; Lv, Z.; Zhangzhong, L. When crops meet machine vision: A review and development framework for a low-cost nondestructive online monitoring technology in agricultural production. *Agric. Commun.* **2024**, *2*, 100029. https://doi.org/10.1016/j.agrcom.2024.100029.
16. Lu, Q.; Li, M. Fault Prediction Method Towards Rolling Element Bearing Based on Digital Twin and Deep Transfer Learning. *Appl. Sci.* **2025**, *15*, 12509.
17. Elbir, A.M.; Papazafeiropoulos, A.K. Hybrid Precoding for Multiuser Millimeter Wave Massive MIMO Systems: A Deep Learning Approach. *IEEE Trans. Veh. Technol.* **2019**, *69*, 552–563. https://doi.org/10.1109/tvt.2019.2951501.
18. Zhong, S.; Feng, H.; Zhang, P.; Xu, J.; Luo, H.; Zhang, J.; Yuan, T.; Huang, L. Deep Learning Based Antenna Selection for MIMO SDR System. *Sensors* **2020**, *20*, 6987. https://doi.org/10.3390/s20236987.
19. Wang, J.; Sun, J.; Fang, W.; Chen, Z.; Liu, Y.; Liu, Y. Deep reinforcement learning for near-field wideband beamforming in STAR-RIS networks. *Front. Inf. Technol. Electron. Eng.* **2024**, *25*, 1651–1663. https://doi.org/10.1631/fitee.2400364.
20. Nie, J.; Cui, Y.; Yang, Z.; Yuan, W.; Jing, X. Near-Field Beam Training for Extremely Large-Scale MIMO Based on Deep Learning. *IEEE Trans. Mob. Comput.* **2024**, *24*, 352–362. https://doi.org/10.1109/tmc.2024.3462960.
21. Farsad, N.; Goldsmith, A. Detection Algorithms for Communication Systems Using Deep Learning. In Proceedings of the 31st Conference on Neural Information Processing Systems (NeurIPS 2017), Long Beach, CA, USA, 4–9 December 2017.
22. Xu, W.; Zhong, Z.; Be'ery, Y.; You, X.; Zhang, C. Joint Neural Network Equalizer and Decoder. In Proceedings of the 2018 International Symposium on Wireless Communication Systems (ISWCS), Lisbon, Portugal, 28–31 August 2018; pp. 1–6. https://doi.org/10.1109/ISWCS.2018.8491056.